analytical chemistry

pubs.acs.org/ac
Article

Localized Shims Enable Low-Field Simultaneous Multinuclear NMR Spectroscopy

Hossein Esmaeilizadshali, Sören Lehmkuhl, Jan Korvink,* and Mazin Jouda*

Cite This: https://doi.org/10.1021/acs.analchem.4c02965
Read Online

ACCESS | Metrics & More | Article Recommendations | Supporting Information

ABSTRACT: This Article introduces a smart localized shimset, integrated with a radiofrequency (RF) microsolenoid and optimized as a single unit to locally achieve high-resolution NMR spectroscopy, as a significant advancement toward achieving parallel NMR spectroscopy. The shimset, consisting exclusively of linear shims, demonstrates the capability to improve NMR line width from 84 to 4 Hz in a 1.05 T preclinical MRI scanner. This enhancement enables the resolution of j-couplings in the sample while requiring a total power of 545 mW. Furthermore, a novel method is presented for concurrently obtaining multinuclear NMR spectra using a single RF channel. This approach allows for the utilization of high-sensitivity NMR signals as a reference to correct field drift, facilitating signal averaging in a permanent magnet NMR scanner that is prone to significant temperature-dependent drift.

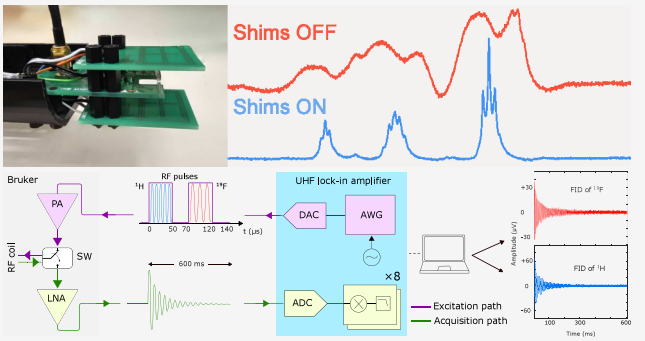

INTRODUCTION

Nuclear magnetic resonance (NMR) spectroscopy stands as a potent technique that relies on the utilization of radio-frequency (RF) electromagnetic radiation to manipulate and detect nuclear spins situated within a static magnetic field B_0. This method is wholly noninvasive. By measuring nuclear spins, which exhibit remarkable sensitivity to their magnetic surroundings, NMR delivers comprehensive insights into the molecular structure and dynamics of a chemical sample, with atomic precision. Consequently, it has become a widely employed analytical technique in the fields of chemistry, biology, the pharmaceutical industry, and the material sciences. For high-resolution spectroscopy, NMR normally requires an exceptionally homogeneous external magnetic field B_0. This uniformity is crucial to ensure that the maximum fluctuations in the magnetic field are kept below the local field perturbations experienced by the spins due to their interactions, commonly referred to as j-couplings. Achieving this high degree of homogeneity is typically accomplished through a set of shim coils carefully designed to replicate the terms of a spherical harmonic expansion,[1−3] which are generally capable of describing any nonuniform magnetic field in a spherical sample. The shimming coils typically used in commercial systems incorporate many terms of the spherical harmonics, up to the fifth order or higher, making them quite complex. This complexity is a major reason why NMR remains a low-throughput spectroscopic technique, only allowing the measurement of one sample at a time. Thus, localized shims, where the shimming coils are integrated with the NMR detector, are crucial for enabling high-throughput parallel multisample NMR. Besides this main advantage, localized shims produce higher fields per current due to their proximity to the sample, allowing more power-efficient shimming. Additionally, they can be optimized so that the shimming sets of multiple samples are orthogonal, permitting independent shimming of each sample.

The literature reports few attempts to integrate localized shims within the RF coils. For instance, Van Meerten et al.[4] introduced the shim-on-chip concept by integrating a 40-wire flat ribbon cable on a stripline NMR detector, aligned perpendicular to the magnet axis. This cable represents a 16-channel 1D shim system capable of generating field gradients along the z-axis in various orders. Tested in a 144 MHz NMR spectrometer, the system achieved a 2.2 Hz line width. The authors in this paper focused on z-axis shimming due to the laterally narrow and extended length of the sample, aligned with the z-axis. While this assumption holds if only sample-induced inhomogeneities are considered, it may not be valid if the B_0 field initially has gradients along the other axes. Additionally, the large number of shim currents needed hinders the scalability of this concept for NMR arrays. In recent work, Cheng et al.[5] demonstrated a two-cell NMR array with

Received: June 9, 2024
Revised: September 18, 2024
Accepted: September 23, 2024

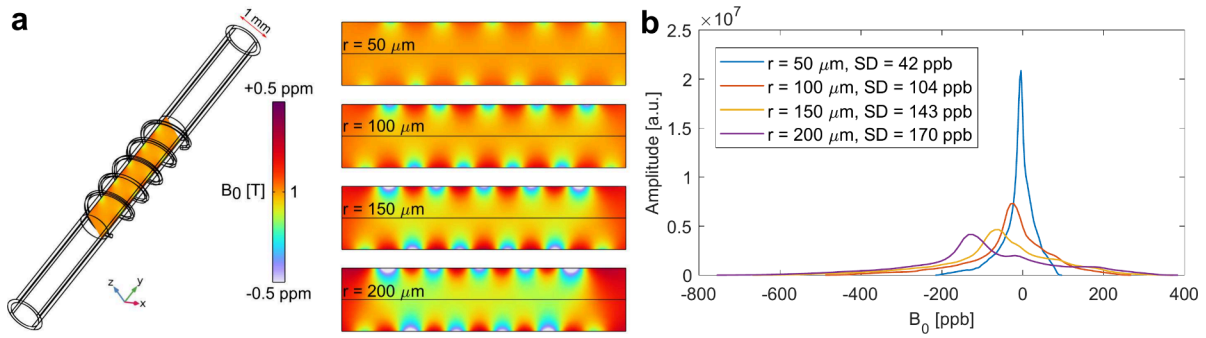

Figure 1. A finite element modeling (FEM) simulation (COMSOL multiphysics) of the B0 field distortion in a sample due to the windings of an RF coil. (a) Simulation geometry includes a copper wire wound around a 1 mm capillary and placed in a 1 T static magnetic field, B0, along the *z*-axis. The field maps are plotted for different wire thicknesses (wire radius, $r \in \{50, 100, 150, 200\ \mu m\}$). (b) A histogram plot of the field inside the sample representing the anticipated NMR spectra and their line widths, denoted by the standard deviation (SD).

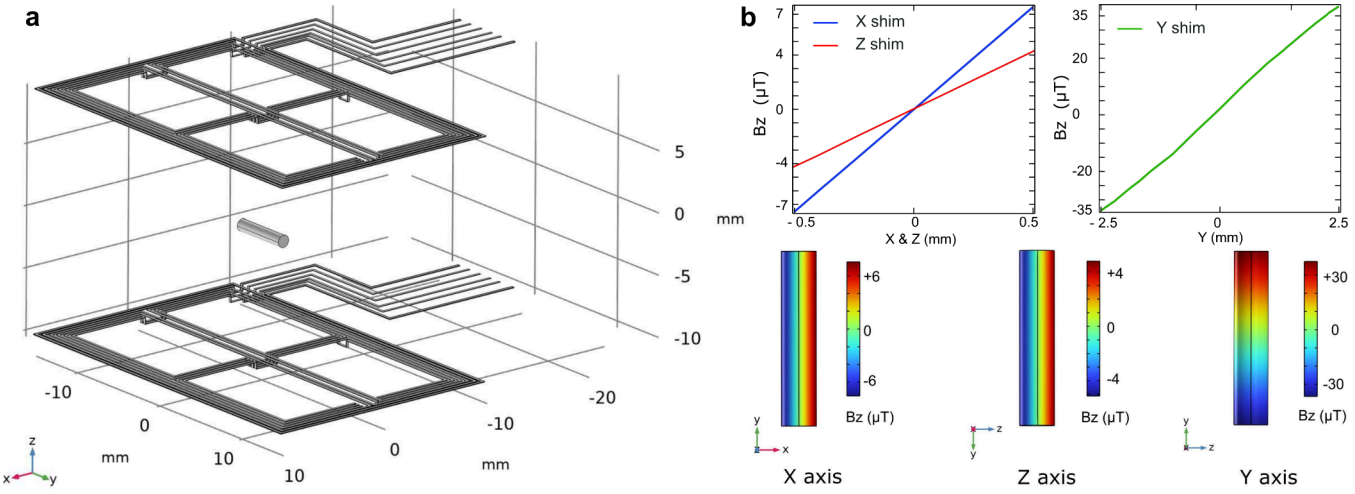

Figure 2. A COMSOL simulation of the designed shims. (a) A 3D model illustrating the sample alongside three linear shim coils (x, y, and z), each constructed from 35 μm thick copper. (b) Field maps of the shims and field profiles within the sample along the three axes.

integrated first-order shims, enabling parallel two-sample NMR spectroscopy. This study highlighted the importance of localized shims for high-throughput spectroscopy. However, it did not optimize the NMR cell (RF detector and shims), resulting in a line width of 28 Hz for the two samples, insufficient to resolve J-couplings. Furthermore, the study used two physical RF transceive channels for the experiment and did not address a scalable, hardware-efficient solution for parallel NMR. Additionally, an integrated shim system comprising nine coils has been introduced to realize a compact spectrometer.[6] In the field of magnetic resonance imaging (MRI), localized shims have been extensively used to enhance the localized B0 homogeneity for imaging and spectroscopic imaging applications. Seminal examples of using localized shim coils in MRI include human brain imaging[7−10] and preclinical imaging.[11,12] Additionally, localized shims proved beneficial for magnetic resonance spectroscopic imaging (MRSI).[13] Furthermore, the literature shows examples of using the RF receive arrays as localized shims, serving as a dual-purpose element.[14,15]

In this paper, we demonstrate how optimizing the NMR detector along with the integrated shimset as a complete unit leads to a smart and efficient shim system capable of achieving high spectroscopic resolution in an imaging magnet. Additionally, we introduce a scalable and hardware-efficient detection scheme that allows for simultaneous multinuclear NMR spectroscopy using a single RF transceive channel. Finally, we detail an optimization method that leverages the simultaneous multinuclear capabilities to enable the detection of low-sensitivity nuclei in a significantly drifting magnet.

SYSTEM DESIGN

Our system, which represents a standalone high-resolution NMR unit, comprises two main components, namely a radiofrequency (RF) coil, and a localized integrated shimset. The design of the RF coil was based on the preselection of a sample holder based on a 1 mm glass capillary, as a good compromise of a sample small enough to reduce the B0 inhomogeneity effects, but sufficiently large to maintain an SNR high enough for shimming. However, the selection of the coil wire thickness was not that straightforward. Hence, a finite element modeling (FEM)-based simulation (COMSOL multiphysics) was conducted to calculate the effect of wire thickness on the B0 field homogeneity within the sample. Figure 1a shows the simulation setup which comprises a copper wire wound around a 1 mm capillary and placed in a 1 T static magnetic field, B0, pointing along the *z*-axis. It additionally depicts the field maps inside the capillary, where the sample is placed, for different wire thicknesses (r is the wire radius, and $r \in \{50\ \mu m, 100\ \mu m, 150\ \mu m, 200\ \mu m\}$). Figure 1b plots a histogram distribution of the field inside the sample volume for the different wire thicknesses, representing the corresponding anticipated NMR spectra. It also calculates the standard

https://doi.org/10.1021/acs.analchem.4c02965
Anal. Chem. XXXX, XXX, XXX−XXX

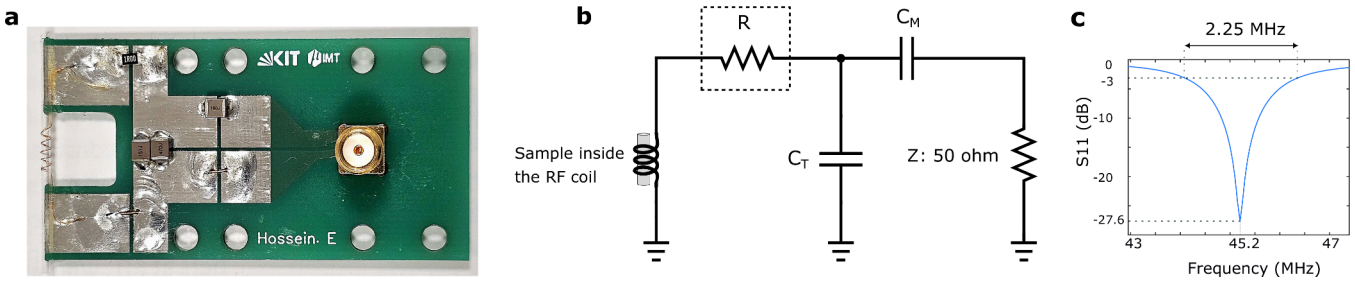

Figure 3. (a) A photograph of the microsolenoid along with the tuning and matching PCB. (b) A schematic diagram of the tuning and matching circuit, highlighting the external resistor, R, that was later used to increase the coil's bandwidth to allow multinuclear NMR. (c) The S_{11} curve of the tuned coil without the external resistor.

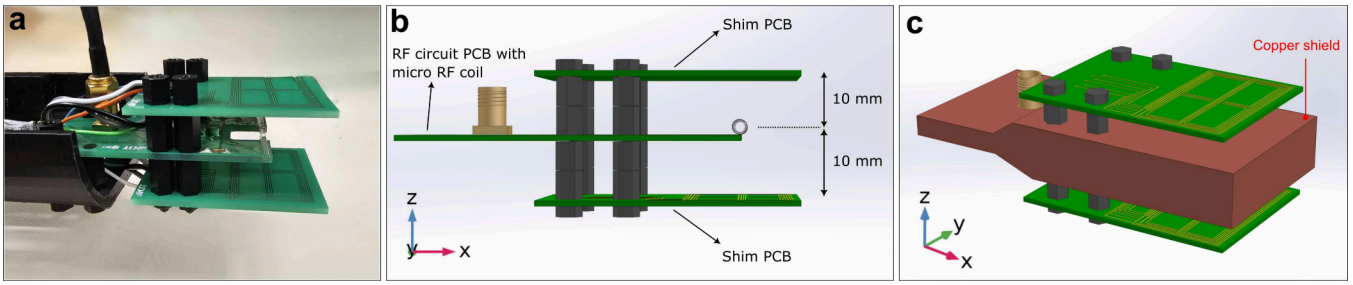

Figure 4. (a) A photograph of the assembled setup including the RF microcoil and the localized linear shimset. (b) A 3D model of the setup showing the distances between the PCBs. (c) The RF section of the circuit was shielded within a grounded copper enclosure to reduce RF interference originating from the shimset and its current drivers.

deviation (SD) of the field for each case. For simplicity and based on the results shown in Figure 1b, only the first-order terms (x, y, and z) were considered here due to their effectiveness in correcting most inhomogeneities of the main magnetic field (B0). However, if higher spectroscopic resolution is needed, additional terms from the well-known spherical harmonics (SH) expansion[16]—a set of orthogonal terms capable of decomposing any inhomogeneous magnetic field near a chosen coordinate position—can be incorporated. The shim coils corresponding to these terms are expected to provide an adequate linear profile over the sample region. For this purpose, we conducted an FEM simulation (COMSOL multiphysics) with a parametric sweep to optimize the geometry of the coils. The simulation geometry along with the simulated field maps of the optimized shims are illustrated in Figure 2.

After ensuring the geometry and the linearity of profiles of x, y, and z through simulation, we started the practical stage of this report. An NMR micro solenoid RF coil was designed and manufactured following the simulation results depicted in Figure 1. It consisted of a copper wire with a 50 μm radius and a capillary with a diameter of 1 mm around which the wire was wound. As shown in Figure 3a, the coil measured 5 mm in length, providing a sensitive sample volume of approximately 4 μL. The wire was wound around the capillary by stacking the ends with a small amount of nonmagnetic liquid glue. Subsequently, the Q-factor and the S-parameters were measured using a Network Analyzer (E5071C ENA), yielding an adequate Q-factor of 40, good enough for high-resolution NMR spectroscopy. The addition of the shim coils and the copper shield slightly lowers the Q-factor to 38 and causes a shift in the resonance frequency, as illustrated in Figure S1 in the Supporting Information. This shift in the resonance was taken into account during the tuning process. Using the Advanced Design System (ADS), the capacitors necessary for tuning and matching the coil at the ^{1}H Larmor frequency (f_L = 45 MHz, corresponding to B_0 = 1.05 T), were determined. According to Figure 3, this circuit includes two sets of capacitors. The first group comprises the tuning capacitance, which is used to precisely adjust the desired frequency. The second group of capacitors form the impedance-matching capacitance, which is used to minimize signal loss or return. The chosen capacitors were then soldered onto the PCB, and the S11 reflection curve of the tuned and matched coil was obtained, as illustrated in Figure 3b, c. The optimized shimming coils were fabricated using commercial printed circuit board (PCB) technology with a 1.55 mm RF4 substrate, and two copper layers of 35 μm thickness. The two shimming PCBs were then mounted on the RF coil's PCB using Teflon screws to maintain a firm and accurate positioning of the shimset relative to the microcoil, see Figure 4. A grounded copper shield was additionally used to enclose the RF PCB, preserving the coil's SNR and eliminating the RF noise of the shimming coils, Figure 4c.

SHIMMING CHARACTERIZATION RESULTS

To assess the performance of the localized shims we filled the sample capillary with a 4 μL Ethanol (CH_3CH_2OH) sample and conducted an NMR experiment with a pulse length of 27 μs, pulse power of 0.1 W, spectral bandwidth of 10 kHz, and acquisition length of 1.4 s. Due to the lack of access over Bruker's shim drivers, an external 3-terminal DC power supply (HMP2030, ROHDE & SCHWARZ) was utilized to drive the localized shims. The shimming process was carried out manually by continuously running a single pulse NMR experiment and iteratively adjusting the shimming currents. This process can readily be automated by employing optimization algorithms such as the Simplex[17] or by adopting recent artificial intelligence (AI)-based methods.[18−20] The shimming results are illustrated in Figure 5 where a ^{1}H NMR

https://doi.org/10.1021/acs.analchem.4c02965
Anal. Chem. XXXX, XXX, XXX−XXX

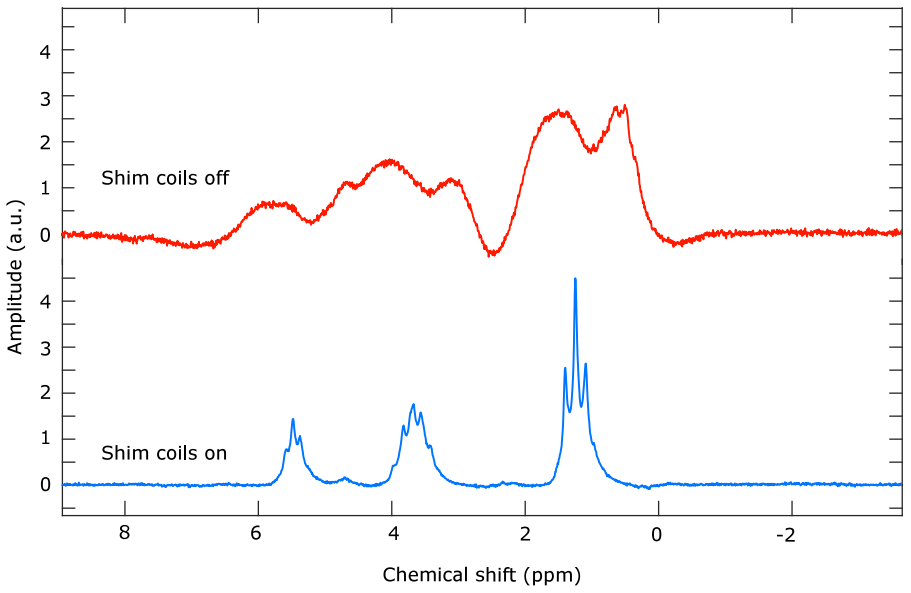

Figure 5. A ^{1}H NMR spectrum of a sample of 4 μL of ethanol acquired for both cases, shims-off (red) and shims-on (blue). The achieved line width after manual shimming is 4 Hz.

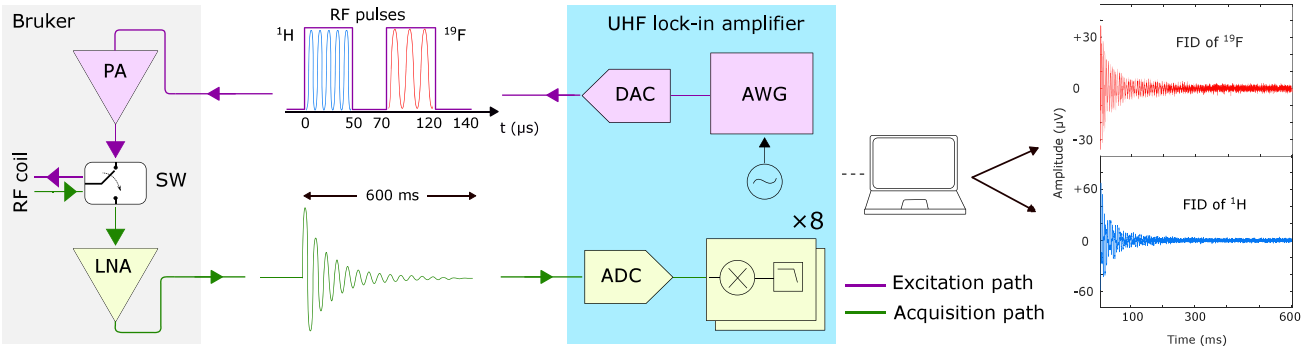

Figure 6. A block diagram of the dual-nucleus experiment setup, illustrating the pathways for excitation and acquisition along with the interface between the UHF lock-in amplifier and the Bruker system. A single RF transceive channel sequentially excites the ^{1}H and ^{19}F spins and then reads their frequency-multiplexed FIDs. The acquisition signal is subsequently digitally demodulated into the FID signals of ^{1}H and ^{19}F. PA: power amplifier, SW: switch, LNA: low-noise amplifier, DAC: digital-to-analog converter, AWG: arbitrary waveform generator, and ADC: analog-to-digital converter.

spectrum of Ethanol is depicted for both cases with "shims OFF" and "shims ON", revealing a best achievable line width of 4 Hz, sufficient to resolve the j-couplings of the sample.

DOUBLE RESONANCE COIL TUNING

A high signal-to-noise (SNR) ratio is key to successful shimming. This becomes particularly challenging in low-field systems due to the naturally weak polarization, especially for nuclei with low gyromagnetic ratios. This problem is even exacerbated when operating in permanent magnets that are prone to significant field drifts in which case signal averaging that is necessary to enhance the SNR becomes infeasible. To address this problem, we introduce a method with which to simultaneously acquire multinuclear NMR signals with a single radiofrequency (RF) transceive channel. With this method, the high receptivity NMR signals, such as ^{1}H for instance, can be utilized to guide the shimming process and additionally track the field drifts so as to enable signal averaging of low receptivity nuclei with no penalty of extra hardware, lower SNR, or elongated measurement time. To validate the proposed method, we decided to conduct a parallel multi-nuclear (^{1}H and ^{19}F) NMR experiment, utilizing the ^{1}H signal as a reference for both shimming and drift adjustment. To carry out this experiment, adjustments were necessary for the RF microcoil to ensure low RF reflection at its port (tuned and matched condition) at the Larmor frequencies of the two nuclei, 45.00 and 42.33 MHz, respectively. Various circuit topologies could achieve this objective,[21,22] broadly falling into two categories: namely, constructing a double resonance circuit using inductor-capacitor (LC) traps or broadening the RF coil's bandwidth to encompass both frequencies.[23,24] The former method, however, proved unsuitable due to the close proximity of the two frequencies, necessitating excessively high-Q traps, which may not be practical. Consequently, we adopted the latter approach, broadening the bandwidth of the tuning and matching circuit depicted in Figure 3b by adding an external resistor in series with the RF coil to reduce its Q-factor. The addition of the resistor lowered the Q-factor of the coil from 38 to 4.7, as demonstrated in Figure S1 of the Supporting Information. This reduction in Q reduces the coil's sensitivity, $B_1/(i\cdot\sqrt{R_c})$, by a factor of

https://doi.org/10.1021/acs.analchem.4c02965
Anal. Chem. XXXX, XXX, XXX−XXX

$\sqrt{Q_{\text{without}-R}/Q_{\text{with}-R}} = 2.84$, where B_1/i is RF magnetic field of the coil per unit current, and R_c is the coil's resistance at the Larmor frequency.[21,25] This modification resulted in the new tuning and matching circuit achieving an S_{11} reflection of −15 dB at the designated frequencies.

MULTINUCLEAR NMR USING A SINGLE RF CHANNEL

Block Diagram of the Experiment Setup. In our experimental setup, we utilized the ultrahigh frequency lock-in amplifier (UHFLI) provided by Zurich Instruments for conducting a parallel multinuclear NMR experiment. The UHFLI is a digital lock-in amplifier featuring two independent hardware units and eight digital demodulators, offering flexible configuration options for assignment to physical channels and demodulation frequencies. Consequently, when employing a single unit, all eight demodulators can be connected to it, enabling the simultaneous and precise extraction of eight distinct frequency bands. For our experiment, we employed a single hardware unit equipped with two digital demodulators to capture the ^{1}H and ^{19}F signals.

The experimental setup, depicted in Figure 6, illustrates the interface between the UHFLI and the analog front-end of the ICON MRI scanner from Bruker. This analog front-end comprises an RF power amplifier for controlling the power of the excitation pulses, an RF low-noise amplifier to enhance reception sensitivity, and an RF switch to toggle between excitation and reception phases while ensuring high isolation of the RF receiver during excitation as well as high isolation of the power amplifier's thermal noise during the reception so as not to overwhelm the weak NMR signals (typically less than 100 μV).

Pulse Sequence. Figure 6 illustrates the pulse sequence employed in this study for conducting a dual-resonance NMR experiment. It involves two successive RF pulses with frequencies of 45.00 and 42.33 MHz, separated by a 20 μs delay, to excite the ^{1}H and ^{19}F nuclear spins, respectively. To ensure phase coherence, two internal oscillators of the UHFLI lock-in amplifier were utilized, with their frequencies set to match the respective ^{1}H and ^{19}F Larmor frequencies. The arbitrary waveform generator (AWG) of the UHFLI was utilized to shape the excitation pulses, modulate the carriers' frequencies of the oscillators, and sequentially route the modulated pulses to the RF output. Following excitation, the resulting NMR free induction decay (FID) represents a frequency multiplexed signal of the ^{1}H and ^{19}F FIDs. Subsequently, this signal undergoes low-noise amplification and is introduced to the RF input of the UHFLI, where it is digitized and subjected to frequency demultiplexing to separate the two FIDs, as depicted in Figure 6.

Multinuclear NMR Results. Acquiring nuclei with a lower gyromagnetic ratio, γ, compared to ^{1}H often requires averaging multiple acquisitions to enhance the signal-to-noise ratio (SNR). However, signal averaging in the available magnet (ICON preclinical MRI system) is impractical due to significant field drift, particularly when shimming is optimized, as achieved with the introduced localized shims. Despite attempts to monitor field drift with high-SNR NMR signals between acquisitions, the drift remains significant. The only viable solution to address this issue is to simultaneously acquire high-SNR signals, to monitor the field drift, alongside the low-SNR ones. To validate this approach, we conducted a parallel (^{1}H and ^{19}F) NMR experiment using a 4 μL sample of C_6F_6 (Hexafluorobenzene) and C_7H_8 (Toluene) mixed in equal volumes, following the experimental setup in Figure 6. The SNR scales proportional to the gyromagnetic ratio[26]

$$\text{SNR} \propto \gamma^3 \tag{1}$$

so that the ^{19}F resonance is expected to be

$$\frac{\text{SNR}_{19\text{F}}}{\text{SNR}_{1\text{H}}} = \left(\frac{40.078 \times 10^6}{42.577 \times 10^6}\right)^3 = 0.81 \tag{2}$$

or 81% of that of ^{1}H. The experiment involved initially using a repeatable single shot of the ^{1}H signal to guide the shimming process. Subsequently, we conducted a parallel experiment by employing the UHFLI internal arbitrary waveform generator (AWG) to produce two consecutive RF pulses with a pulse width of 50 μs and a separation of 20 μs between them, Figure 6. These pulses modulated two carrier signals with frequencies of 45 MHz (^{1}H) and 42.33 MHz (^{19}F), respectively. The excitation pulses were then amplified using Bruker's power amplifier and applied to the RF coil via the RF switch. Following excitation, the detected NMR signal (a frequency multiplexed signal containing the ^{1}H and ^{19}F NMR free induction decay signals) was amplified using Bruker's low-noise amplifier (LNA), digitized by the UHFLI, and processed by two of its internal digital demodulators operating at 45 and 42.33 MHz, respectively. The bandwidth of the digital demodulators was set to 10 kHz for both channels and the repetition time was set to 1 s.

Figure 7 illustrates the results of acquiring 16 scans of simultaneous ^{1}H (Figure 7a) and ^{19}F (Figure 7b) NMR spectroscopy. Despite the relatively short repetition time of 1 s, one can clearly see the significant field drift between acquisitions, which, if left uncorrected, results in considerable spectral line broadening and consequently an intolerable loss of spectroscopic resolution. Simply correcting the field drift using a high-SNR signal is insufficient for successful averaging of low-SNR signals. This inadequacy arises because the phase response of the NMR receiver varies with the Larmor frequency (i.e., the field value). Consequently, each acquisition exhibits an arbitrarily different phase, rendering it impossible to constructively sum the acquisitions even after correcting for frequency drift. To address this challenge, we developed a generalized method using the optimization toolbox in Matlab. Tailored for NMR simultaneous acquisitions of multiple nuclei, this method necessitates at least one nucleus exhibiting a sufficiently high SNR to monitor the field drift. In the example of parallel spectroscopy involving ^{1}H and ^{19}F signals illustrated in Figure 7, we designate the ^{1}H signal as the high-SNR reference for measuring field drift, while considering the ^{19}F signal as the low-SNR target. Consequently, the method enables the successful summation of the ^{19}F acquisitions through the procedure below. The unmodified ^{19}F FID is given by

$$r(t) = x + j{\cdot}y \tag{3}$$

^{19}F FID after frequency correction:

$$r_1(t) = r{\cdot}e^{j{\cdot}2\pi{\cdot}f_H{\cdot}(\frac{\gamma_{19\text{F}}}{\gamma_{1\text{H}}}){\cdot}t} \tag{4}$$

where f_H is the frequency drift measured using the ^{1}H signal. Consequently, the optimization objective function is

https://doi.org/10.1021/acs.analchem.4c02965
Anal. Chem. XXXX, XXX, XXX−XXX

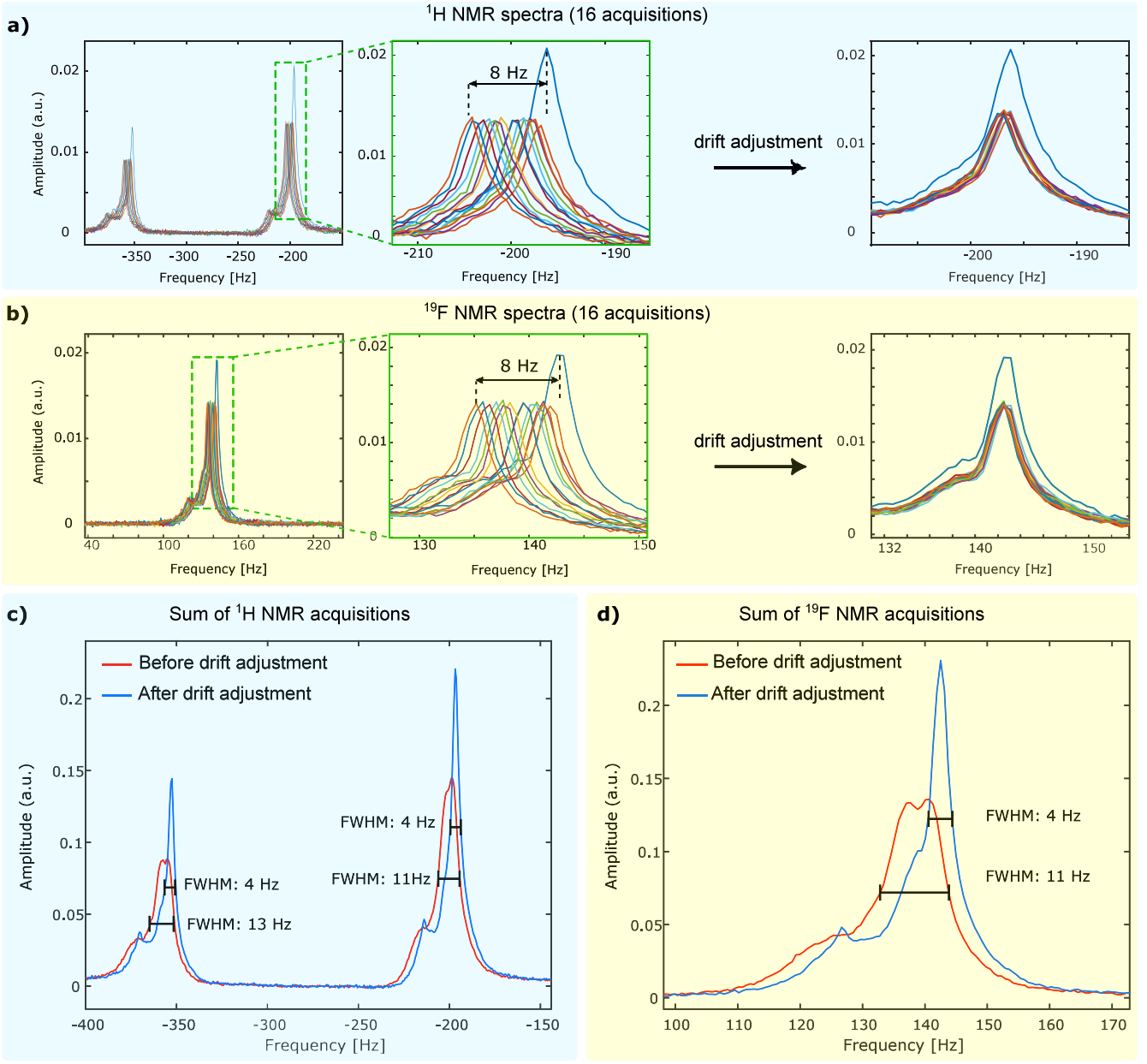

Figure 7. Sixteen simultaneous acquisitions of (a) ^{1}H and (b) ^{19}F NMR spectra revealed a significant magnetic field drift, even with a 1 s repetition time. The sums of the 16 acquisitions before and after the optimized drift adjustment for (c) ^{1}H and (d) ^{19}F are shown.

$$\max\left\{\sum_{i=1}^{n}\sum \Re(\mathcal{F}(r_1(t)))\cdot e^{j\cdot PH_i)}\right\} \quad (5)$$

where $PH_i = PH0_i + PH1_i \cdot f$ is the phase correction term of the i-th acquisition, including the zero-order and first-order coefficients of the truncated expansion terms $PH0_i$ and $PH1_i$. The symbol n represents the number of acquisitions. The optimization objective function aims to maximize the integration of the sum of n NMR spectra after applying phase correction. The optimization variables, in this case, are the phase correction coefficients, $PH0_i$ and $PH1_i$ with $i\in\{1,2,\cdots,n\}$. The results of applying this method of frequency drift adjustment and optimized phase correction to successfully average 16 NMR scans are demonstrated in Figure 7c,d. In this figure, we only considered the zero-order phase correction, $PH0_i$. The figure shows the precise summation of the NMR signals and the successful recovery of the NMR spectral resolution in a significantly drifting magnet.

DISCUSSION AND CONCLUSIONS

In this paper, we present a method to design and optimize localized shimsets for integration with NMR detectors, enabling high-resolution NMR spectroscopy within a permanent low-field MRI magnet. Our findings highlight that optimizing the RF coil in conjunction with the shims as an entire system is crucial for achieving high-resolution spectroscopy while minimizing the number of shims needed. By applying this approach, we demonstrated that an NMR detector with an optimized geometry and wire thickness, along with a geometrically optimized shimset consisting only of first-order shims, can improve the NMR line width from 84 to 4 Hz, allowing the resolution of J-couplings in an imaging magnet.

https://doi.org/10.1021/acs.analchem.4c02965
Anal. Chem. XXXX, XXX, XXX−XXX

However, the achieved line width does not fully reflect the true performance of the introduced system (RF detector + shimset) due to significant magnet drift observed during the shimming process. Demonstrating the capability of localized shims to perform NMR spectroscopy in a wide-bore MRI magnet represents a significant advancement toward high-throughput NMR spectroscopy, as the available space in the magnet can easily accommodate more of these compact systems (RF coil + local shimset), particularly given the potential for further miniaturization enabled by the 2D planar structure of the shims.

As this system offers a solution for multisample high-resolution NMR arrays, the hardware complexity arising from the need for a separate RF transceive channel for each NMR detector and nucleus becomes a major barrier to high-throughput NMR spectroscopy. To address this, we introduced a novel excitation and detection scheme based on digital lock-in detection, which enables multinuclear NMR using a single RF transceive channel. While we demonstrated this detection scheme in a dual-nuclei NMR experiment, it has the capacity to acquire signals from up to eight nuclei with a single RF channel. Leveraging the ability to acquire multinuclear NMR signals simultaneously, we developed an optimization algorithm that allows for the averaging of low-sensitivity NMR signals in a drifting field without the need for an additional lock channel. The proposed postprocessing-based drift correction method is advantageous in the sense that it, unlike old methods, does not require a dedicated reference to be added to the sample, which might not be favorable for biological samples for instance, nor does it require a dedicated reference sample with a separate RF channel as a lock channel, as is the case in current spectrometers. So any high-sensitivity nucleus in the sample can be exploited to monitor the field drift and correct it in the postprocessing.

From the hardware side, there are virtually no limitations except if the field drift causes second or higher-order phase errors in the spectra. The main limitation of this method, however, is the computational power of the computer where the optimization routine is executed. For instance, correcting the field drift and the zero-order phase to average 16 NMR acquisitions takes 3.2 s using the Matlab optimization toolbox on a PC with an Intel Core i7−10510u CPU @1.8 GHz 2.3 GHz, and 16 GB RAM. This time can be further reduced by characterizing the phase response of the spectrometer over the expected field/frequency drift range and using this information to narrow down the search domain of the phase during the optimization.

With its post hoc ability to correct the field drift, this method, unlike conventional lock mechanisms, does not need a Z_0 shim coil to correct the field which relaxes its hardware requirements. Nevertheless, the hardware-efficient detection scheme introduced in the paper can be used to perform conventional field-drift correction by using one of the high-sensitivity nuclei available in the sample to drive the Z_0 shim coil through the internal PID (proportional-integral-derivative) controller of the UHFLI. In this case, all that is needed is to integrate a Z_0 shim coil onto the NMR cell (sample + RF coil + shims) so that the field drift can be locally corrected in real-time for every cell.

■ ASSOCIATED CONTENT

Supporting Information

The Supporting Information is available free of charge at https://pubs.acs.org/doi/10.1021/acs.analchem.4c02965.

Information ont he effect of shim coils, the copper shielding, and the added resistor on the Q-factor of the coil and a photo of the setup with the copper shield (PDF)

■ AUTHOR INFORMATION

Corresponding Authors

Jan Korvink − *Institute of Microstructure Technology, Karlsruhe Institute of Technology, D-76344 Eggenstein-Leopoldshafen, Germany;* orcid.org/0000-0003-4354-7295; Email: jan.korvink@kit.edu

Mazin Jouda − *Institute of Microstructure Technology, Karlsruhe Institute of Technology, D-76344 Eggenstein-Leopoldshafen, Germany;* orcid.org/0000-0002-1226-1174; Email: mazin.jouda@kit.edu

Authors

Hossein Esmaeilizadshali − *Institute of Microstructure Technology, Karlsruhe Institute of Technology, D-76344 Eggenstein-Leopoldshafen, Germany*

Sören Lehmkuhl − *Institute of Microstructure Technology, Karlsruhe Institute of Technology, D-76344 Eggenstein-Leopoldshafen, Germany;* orcid.org/0000-0002-1321-7677

Complete contact information is available at: https://pubs.acs.org/10.1021/acs.analchem.4c02965

Notes

The authors declare the following competing financial interest(s): J.G.K. is a shareholder of Voxalytic GmbH, a startup company that produces microscale NMR devices. The other authors declare no competing interests.

■ ACKNOWLEDGMENTS

This work was funded by the Deutsche Forschungsgemeinschaft (DFG, German Research Foundation), SFB 1527/1-project-ID 454252029 (HyPERiON). This work was additionally supported by the Helmholtz Association Research Area Information, Materials Systems Engineering, Topic 5 Materials Information Discovery, CRC SFB-1537 ECOSENSE, and the Karlsruhe Institute of Technology. The authors additionally acknowledge the KIT-Publication Fund.

■ REFERENCES

(1) Golay, M. J. *Rev. Sci. Instrum.* **1958**, *29*, 313−315.
(2) Anderson, W. A. *Rev. Sci. Instrum.* **1961**, *32*, 241−250.
(3) Roméo, F.; Hoult, D. I. *Magn. Reson. Med.* **1984**, *1*, 44−65.
(4) van Meerten, S. G. J.; van Bentum, P. J. M.; Kentgens, A. P. M. *Anal. Chem.* **2018**, *90*, 10134−10138.
(5) Cheng, Y.-T.; Jouda, M.; Korvink, J. *Sci. Rep.* **2022**, *12*, 14149.
(6) Price, J. C.; Jonkman, C. Shim coils and shimming miniaturized nuclear magnetic resonance magnets. US 8729898 B2, 2014.
(7) Juchem, C.; Umesh Rudrapatna, S.; Nixon, T. W.; de Graaf, R. A. *Neuroimage* **2015**, *105*, 462−472.
(8) Juchem, C.; Nixon, T. W.; McIntyre, S.; Boer, V. O.; Rothman, D. L.; de Graaf, R. A. *Journal of magnetic resonance* **2011**, *212*, 280−288.
(9) Juchem, C.; Nixon, T. W.; McIntyre, S.; Rothman, D. L.; de Graaf, R. A. *Magnetic Resonance in Medicine: An Official Journal of the*

International Society for Magnetic Resonance in Medicine **2010**, *63*, 171−180.
(10) Meneses, B. P.; Stockmann, J. P.; Arango, N.; Gapais, P.-F.; Giacomini, E.; Mauconduit, F.; Gras, V.; Boulant, N.; Vignaud, A.; Luong, M.; et al. *Neuroimage* **2022**, *261*, 119498.
(11) Juchem, C.; Herman, P.; Sanganahalli, B. G.; Brown, P. B.; McIntyre, S.; Nixon, T. W.; Green, D.; Hyder, F.; de Graaf, R. A. *NMR in Biomedicine* **2014**, *27*, 897−906.
(12) Juchem, C.; Brown, P. B.; Nixon, T. W.; McIntyre, S.; Rothman, D. L.; de Graaf, R. A. *Magn. Reson. Med.* **2011**, *66*, 893−900.
(13) Esmaeili, M.; Stockmann, J.; Strasser, B.; Arango, N.; Thapa, B.; Wang, Z.; van der Kouwe, A.; Dietrich, J.; Cahill, D. P.; Batchelor, T. T.; et al. *Sci. Rep.* **2020**, *10*, 15029.
(14) Stockmann, J. P.; Witzel, T.; Keil, B.; Polimeni, J. R.; Mareyam, A.; LaPierre, C.; Setsompop, K.; Wald, L. L. *Magn. Reson. Med.* **2016**, *75*, 441−451.
(15) Stockmann, J. P.; Arango, N. S.; Witzel, T.; Mareyam, A.; Sappo, C.; Zhou, J.; Jenkins, L.; Craven-Brightman, L.; Milshteyn, E.; Davids, M.; et al. *Magn. Reson. Med.* **2022**, *87*, 1074−1092.
(16) Golay, M. J. E. *Rev. Sci. Instrum.* **1958**, *29*, 313−315.
(17) Yao, K.; Liu, M.; Zheng, Z.; Shih, T.; Xie, J.; Sun, H.; Chen, Z. *IEEE Transactions on Instrumentation and Measurement* **2021**, *70*, 1−12.
(18) Becker, M.; Jouda, M.; Kolchinskaya, A.; Korvink, J. G. *J. Magn. Reson.* **2022**, *336*, 107151.
(19) Becker, M.; Lehmkuhl, S.; Kesselheim, S.; Korvink, J. G.; Jouda, M. *J. Magn. Reson.* **2022**, *345*, 107323.
(20) Becker, M.; Cheng, Y.-T.; Voigt, A.; Chenakkara, A.; He, M.; Lehmkuhl, S.; Jouda, M.; Korvink, J. G. *Sci. Rep.* **2023**, *13*, 17983.
(21) Mispelter, J.; Lupu, M.; Briguet, A. *Nmr Probeheads for Biophysical and Biomedical Experiments: Theoretical Principles & Practical Guidelines*, 1st ed.; Imperial College Press, 2006.
(22) Davoodi, H.; Jouda, M.; Korvink, J. G.; MacKinnon, N.; Badilita, V. *Prog. Nucl. Magn. Reson. Spectrosc.* **2019**, *112*−*113*, 34−54.
(23) Fratila, R. M.; Gomez, M. V.; Sỳkora, S.; Velders, A. H. *Nat. Commun.* **2014**, *5*, 3025.
(24) Anders, J.; Velders, A. H. Microcoils for broadband multinuclei detection. In *Micro and Nano Scale NMR: Technologies and Systems*; Wiley, **2018**; p 265.
(25) Webb, A. G. *Prog. Nucl. Magn. Reson. Spectrosc.* **1997**, *31*, 1−42.
(26) Korvink, J. G.; MacKinnon, N.; Badilita, V.; Jouda, M. *J. Magn. Reson.* **2019**, *306*, 112−117.

https://doi.org/10.1021/acs.analchem.4c02965
Anal. Chem. XXXX, XXX, XXX−XXX